Disentangling the effects of Alzheimer's and small vessel disease on white matter fibre tracts

Anna Dewenter,[1] Mina A. Jacob,[2] Mengfei Cai,[2] Benno Gesierich,[1,3] Paul Hager,[1,4] Anna Kopczak,[1] Davina Biel,[1] Michael Ewers,[1,5] Anil M. Tuladhar,[2] Frank-Erik de Leeuw,[2] Martin Dichgans,[1,5,6] Nicolai Franzmeier[1,†] and Marco Duering[1,3,†] for the SVDs@target Consortium and Alzheimer's Disease Neuroimaging Initiative (ADNI)

1 Institute for Stroke and Dementia Research (ISD), University Hospital, LMU Munich, Germany

2 Department of Neurology, Donders Institute for Brain, Cognition and Behaviour, Radboud University Medical Center, Nijmegen, The Netherlands

3 Medical Image Analysis Center (MIAC) and Department of Biomedical Engineering, University of Basel, Basel, Switzerland

4 Institute for AI and Informatics in Medicine, Klinikum rechts der Isar, Technical University of Munich, Munich, Germany

5 German Center for Neurodegenerative Disease (DZNE), Munich, Germany

6 Munich Cluster for Systems Neurology (SyNergy), Munich, Germany

Correspondence to: Marco Duering
Medical Image Analysis Center (MIAC AG)
Marktgasse 8, CH-4051 Basel, Switzerland
E-mail: marco.duering@miac.ch

[†]**These authors contributed equally to this work.**

Abstract

Alzheimer's disease and cerebral small vessel disease are the two leading causes of cognitive decline and dementia and co-exist in most memory clinic patients. White matter damage as assessed by diffusion MRI is a key feature in both Alzheimer's and cerebral small vessel disease. However, disease-specific biomarkers of white matter alterations are missing. Recent advances in diffusion MRI operating on the fixel level (*fi*ber population within a vo*xel*) promise to advance our understanding of disease-related white matter alterations. Fixel-based analysis allows to derive measures of both white matter microstructure, measured by fiber density, and macrostructure, measured by fiber-bundle cross-section. Here, we evaluated the capacity of these state-of-the-art fixel metrics to disentangle the effects of cerebral small vessel disease and Alzheimer's disease on white matter integrity.

We included three independent samples (total *n*=387) covering genetically defined cerebral small vessel disease and age-matched controls, the full spectrum of biomarker-confirmed Alzheimer's disease including amyloid- and tau-PET negative controls and a validation sample with presumed mixed pathology. In this cross-sectional analysis, we performed group comparisons between patients and controls and assessed associations between fixel metrics within main white matter tracts and imaging hallmarks of cerebral small vessel disease (white matter hyperintensity volume, lacune and cerebral microbleed count) and Alzheimer's disease (amyloid- and tau-PET), age and a measure of neurodegeneration (brain volume).

Our results showed that i) fiber density was reduced in genetically defined cerebral small vessel disease and strongly associated with cerebral small vessel disease imaging hallmarks, ii) fiber-bundle cross-section was mainly associated with brain volume, and iii) both fiber density and fiber-bundle cross-section were reduced in the presence of amyloid, but not further exacerbated by abnormal tau deposition. Fixel metrics were only weakly associated with amyloid- and tau-PET.

Taken together, our results in three independent samples suggest that fiber density captures the effect of cerebral small vessel disease, while fiber-bundle cross-section is largely determined by neurodegeneration. The ability of fixel-based imaging markers to capture distinct effects on white matter integrity can propel future applications in the context of precision medicine.

Running title: Disentangling effects on white matter

Keywords: Alzheimer's disease; cerebral small vessel disease; fixel-based analysis; diffusion magnetic resonance imaging; CADASIL

Abbreviations: Aβ = amyloid-beta; AD = Alzheimer's disease; ADNI = Alzheimer's Disease Neuroimaging Initiative; BrainV = brain volume; CADASIL = Cerebral Autosomal Dominant Arteriopathy with Subcortical Infarcts and Leukoencephalopathy; fixel = (specific) fiber population within a voxel; SVD = cerebral small vessel disease; WMH = white matter hyperintensity.

Introduction

Alzheimer's disease (AD) and cerebral small vessel disease (SVD) are the two most frequent causes of dementia.[1,2] AD is a proteinopathy characterized by the cortical accumulation of amyloid-beta (Aβ) plaques and neurofibrillary tau tangles that lead to neurodegeneration, which can be assessed using PET and MRI.[3] In contrast, SVD is associated with pathologic alterations of small penetrating vessels that manifest on MRI mainly as white matter hyperintensities, lacunes and cerebral microbleeds.[4,5] While AD and SVD are distinct diseases with different etiologies and pathomechanisms, the majority of patients who seek clinical care in memory clinics present with both AD- and SVD-related brain alterations to varying degrees. Histopathology studies have shown that up to 80% of patients with prodromal AD show cerebrovascular alterations upon autopsy.[6] This suggests substantial overlap between both disease entities in clinical populations, probably due to shared risk factors.[6–8] Hence, there is a great need for biomarkers that capture both AD and SVD and describe the extent and contribution of each disease within the individual patient.

In recent years, diffusion MRI has evolved as the method of choice to quantify white matter alterations in SVD, with most studies relying on diffusion tensor imaging.[9,10] Diffusion alterations in the white matter are also frequently observed across the AD continuum.[11,12] Global white matter diffusion metrics seem largely determined by SVD-related white matter damage, masking any white matter damage that might occur due to AD pathology.[13] Studies using regions-of-interest or tract-based analysis suggest different spatial patterns of diffusion MRI alterations in AD and SVD, which warrants to study regional effects on white matter fiber tracts.[14,15] However, specific biomarkers for AD-related and SVD-related white matter damage are still missing.

A potential reason why previous diffusion models failed to disentangle white matter alterations due to different pathologies is their incapacity to account for the complex anatomy of brain white matter.[16] Histology studies show that the brain's white matter architecture is highly complex with up to 98% of the white matter consisting of multiple fibers with crossing fiber orientations.[17,18] State-of-the-art constrained spherical deconvolution algorithms yield promise since they allow to

derive diffusion measures specific to underlying fiber populations, i.e. on the *fixel* level (*fi*ber population within a vo*xel*) instead of the voxel level (**Figure 1**).[19] Using this framework, one can simultaneously derive tract-specific measures of fiber density and fiber-bundle cross-section. Fiber density is a fixel-specific feature of white matter *micro*structure, approximately proportional to the total intra-axonal volume.[20] Fiber-bundle cross-section is a fixel-specific *macro*scopic feature, presumably reflecting the accumulated axon loss.[19,21]

The first fixel-based study in clinical AD and mild cognitive impairment reported reductions in both fiber density and fiber-bundle cross-section of main fiber tracts compared with cognitively healthy controls.[22] However, it remains elusive, 1) whether amyloid and tau pathology is associated with fiber density or fiber-bundle cross-section and 2) whether this association is altered in sporadic AD with comorbid SVD. Eventually, the ability of fiber density and fiber-bundle cross-section to describe and disentangle the effects of SVD and AD pathology on white matter integrity within the same patient has not been explored so far.

To address the need for disease-specific markers, the first aim of this study was to assess the effects of both SVD and biomarker-confirmed AD on both fiber density and fiber-bundle cross-section of major white matter fiber tracts compared with age-matched controls. Our second aim was to explore the relationship between well-established SVD MRI and AD PET imaging hallmarks with tract-specific measures of fiber density and fiber-bundle cross-section. We addressed these aims using three independent samples (total *n*=387) covering genetically defined SVD (cerebral autosomal dominant arteriopathy with subcortical infarcts and leukoencephalopathy [CADASIL]) and age-matched controls, sporadic AD with full amyloid- and tau-PET-based biomarker characterization including controls without amyloid and tau pathology as well as a validation sample with mixed pathology. We combined conventional MRI markers and PET data with state-of-the-art fixel-based analyses of advanced diffusion MRI data. Our main goal was to disentangle white matter damage due to AD and SVD using fixel-based metrics, opening the road for disease-specific white matter characterization towards precision medicine.

Materials and methods

Participants

We included three independent samples with 3 Tesla multi-shell diffusion MRI (**Figure 2)**. First, to study the effect of SVD in isolation, we included patients with genetically defined SVD and age-matched controls. Second, the effect of AD was studied across the full spectrum of sporadic AD pathology, ranging from age-matched controls without evidence of amyloid or tau pathology (Aβ–T–), to patients with amyloid pathology only (Aβ+T–), and patients with both amyloid and tau pathology (Aβ+T+). Lastly, we used a third study sample with presumed mixed pathology for independent validation.

Study protocols were in accordance with the declaration of Helsinki and approved by local ethics committees. Written informed consent was obtained from all participants.

Small vessel disease sample

We included in total 95 participants with identical MRI acquisition on the same scanner from a single-center cohort in Munich[10] (*n*=79) and the ZOOM@SVDs study[23] (*n*=16), of which 73 were patients with genetically defined SVD (CADASIL), and 22 were healthy controls matched for age and sex on the group level. CADASIL patients were symptomatic, but in an early disease stage (i.e., functionally independent).

Alzheimer's disease sample

Participants from the Alzheimer's Disease Neuroimaging Initiative 3 (ADNI) database were selected based on availability of multi-shell diffusion MRI and structural MRI, as well as ^{18}F-florbetapir or ^{18}F-florbetaben amyloid-PET and ^{18}F-flortaucipir tau-PET within 6 months of the MRI visit (*n*=106).[24] 17 participants were excluded due to relevant diffusion MRI protocol deviations (*n*=16) or a cropped field of view (*n*=1). Controls were matched for age and sex on the group level.

We used a biological definition of AD following NIA-AA guidelines[3] and assigned participants as Aβ+ when surpassing a global pre-established Aβ positivity standardized uptake value ratio (SUVR) threshold of 1.11 for ^{18}F-florbetapir and 1.08 for ^{18}F-florbetaben amyloid-PET.[25] Tau

positivity was assigned when surpassing a pre-established ^{18}F-flortaucipir SUVR threshold of 1.3 in any of the pre-defined Braak stage regions (Braak1, Braak3, Braak3/4, Braak4, Braak5, Braak5/6, Braak6).[26,27] Of note, the hippocampus (i.e. Braak2) was excluded from all analyses, due to relevant off-target binding of the ^{18}F-flortaucipir tracer in the medial temporal lobe. Since our main interest was in the neuropathological effects of amyloid and tau pathology on white matter tissue integrity, we used exclusively the biological definition of Alzheimer's disease and did not take clinical status into account. We included 71 participants, of which 34 controls had no biomarker evidence for AD pathology (Aβ–T–) and 37 Aβ+ individuals across the AD spectrum (19 Aβ+T–, 18 Aβ+T+).

Validation sample

We selected participants from the 3rd follow-up visit (approx. 14 years after baseline) of the RUN DMC study[28] (Radboud University Nijmegen Diffusion tensor and Magnetic resonance imaging Cohort), based on the availability of multi-shell diffusion MRI (*n*=228). We excluded 6 participants with infarcts of non-SVD etiology and 1 participant due to an MRI protocol deviation, resulting in a final sample of 221 participants. While the cohort recruited non-demented elderly with SVD, neurodegenerative pathologies were not excluded and during the long-term follow-up, some participants were in fact diagnosed with AD dementia (**Figure 2**).[29] Therefore, we refer to this sample as validation sample with presumed mixed pathology. However, data on amyloid or tau, either PET or fluid biomarkers, were not available for these participants.

MRI acquisition and conventional MRI markers

Full sequence parameters are shown in **Supplementary Table e-1**. Sequence parameters varied per study, but included 3D T1-weighted, 3D fluid-attenuated inversion recovery (FLAIR) and 3D gradient echo (T2*-weighted) sequences to assess conventional MRI markers (white matter hyperintensity volume [WMHV], lacune and cerebral microbleed count, brain volume [BrainV]) as well as a multi-shell diffusion MRI sequence. Conventional MRI markers were quantified according to consensus criteria.[4] All volumes were normalized to the intracranial volume (e.g. WMHV/intracranial volume).

Small vessel disease sample

MRI scans were performed on a single 3 Tesla scanner (Magnetom Skyra with 64-channel head/neck coil; Siemens Healthineers, Erlangen, Germany). The diffusion MRI protocol comprised a multi-band echo planar imaging multi-shell diffusion-weighted imaging sequence (repetition time 3800 ms, echo time 105 ms, diffusion-encoding directions: 30 x b = 1000 s/mm^2 and 60 x b = 2000 s/mm^2, 10 b = 0 images, multi-band factor 3). One b = 0 image with inverted phase-encoding direction was acquired for correction of susceptibility-induced distortions during processing.[30,31] Details on the calculation of conventional MRI markers have been described previously.[10]

Alzheimer's disease sample

MRI scans were performed on different (in total 13) 3 Tesla scanners (Magnetom Prisma or Magnetom Prisma Fit with 20-, 32- or 64-channel coils; Siemens Healthineers). The diffusion MRI protocol comprised a multi-band echo planar imaging multi-shell diffusion-weighted sequence (repetition time 3400 ms, echo time 71 ms, diffusion-encoding directions 48 x b = 1000 s/mm^2 and 60 x b = 2000 s/mm^2, 13 b = 0 images, multi-band factor 3).

White matter hyperintensities were segmented using a deep-learning algorithm based on multi-dimensional gated recurrent units (https://github.com/zubata88/mdgru).[32] An expert rater blinded to biomarker status determined the number of lacunes on FLAIR and T1-weighted images and the number of cerebral microbleeds on T2*-weighted images. Brain and intracranial volumes were estimated from the T1-weighted image with the cross-sectional Sequence Adaptive Multimodal SEGmentation (SAMSEG) Pipeline (FreeSurfer software suite, version 7.1).[33]

Validation sample

MRI scans were performed on a single 3 Tesla scanner (Magnetom Prisma with 32-channel head coil; Siemens Healthineers). The diffusion MRI protocol comprised a multi-band echo planar imaging multi-shell diffusion-weighted imaging sequence (repetition time 3220 ms, echo time 74 ms, diffusion-encoding directions 30 x b = 1000 s/mm^2 and 60 x b = 3000 s/mm^2, 10 b = 0 images, multi-band factor 3). One b = 0 image with inverted phase-encoding direction was acquired for correction of susceptibility-induced distortions during processing. Details on the calculation of conventional MRI markers have been described previously.[34,35]

Diffusion MRI preprocessing

Preprocessing steps included visual quality control, Marchenko-Pastur principal component analysis-based denoising, Gibbs artefact removal, and dynamic correction for susceptibility-induced distortions, eddy current-induced distortions, as well as head motion using tools from MRtrix3 (www.mrtrix.org/, version 3.0.0, dwidenoise,[36–39] mrdegibbs[39,40]) and the Functional Magnetic Resonance Imaging of the Brain Software Library (FSL, version 6.0.1, topup,[30,31] eddy[41] including state-of-the art replacement of outliers,[42] usage of the slice-to-volume motion model[43] and susceptibility-by-movement correction[44]). Due to unavailability of an unweighted diffusion image with reversed phase-encoding in the AD sample, we used Synb0-DISCO to synthesize an unweighted diffusion image without susceptibility-induced distortion from the T1-weighted image.[45,46] Other than this single step, preprocessing was kept identical across the three samples.

Tract-specific fixel-based analysis

We followed the fixel-based analysis pipeline recommended by the developers using multi-tissue constrained spherical deconvolution to compute fiber orientation distributions (FODs).[21,47] Fixel-based analyses were computed independently for each sample. Diffusion data was corrected for bias fields followed by a global DWI intensity normalization between subjects of each sample, yielding diffusion weighted images with identical b=0 white matter median intensity value. Response functions were estimated for each participant using the 'dhollander' algorithm,[48] based on which the mean response functions were computed. Remaining steps included upsampling to 1.25 mm voxel size, estimation of the fiber-orientation distributions using the group response functions ('msmt_csd' algorithm) and intensity normalization. Next, study-specific FOD templates were calculated by randomly selecting representative participants, i.e. 15 controls & 15 CADASIL patients for the SVD sample, 15 Aβ–T– & 7 Aβ+T– & 8 Aβ+T+ for the AD sample and 30 study participants from the validation sample. Subject-specific FOD images were registered to the FOD template, whereafter fixels were segmented and corresponding metrics of apparent fiber density, fiber-bundle cross-section and a combined measure of fiber density and cross-section were derived. Since our main interest was to find disease-specific metrics for white matter damage, we focused on the primary metrics fiber density and fiber-bundle cross-section

(but conducted supplementary analyses on the combined metric fiber density and bundle cross-section).

Next, we used TractSeg, a deep learning-based framework for automated white matter bundle segmentation, to segment the FOD template into 72 anatomically well-established white matter fiber tracts.[49] To reduce the number of comparisons, we averaged tract measures for left and right hemispheres. Also, to further reduce the number of regions-of-interest, we excluded the tracts located in the cerebellum – since it is up to date unclear how SVD and AD manifest in this brain area – as well as the fornix due to unavoidable CSF partial-volume effects. In addition, we excluded striatal projections from our analyses, due to a high anatomical overlap with thalamic projections. This resulted in 29 white matter fiber tracts (**Figure 3**, from top left): arcuate fasciculus (AF), uncinate fasciculus (UF), inferior fronto-occipital fasciculus (IFOF), middle longitudinal fasciculus (MLF), inferior longitudinal fasciculus (ILF), superior longitudinal fasciculus I to III (SLF-I, SLF-II, SLF-III), thalamo-prefrontal (T-PREF), thalamo-premotor (T-PREM), thalamo-precentral (T-PREC), thalamo-postcentral (T-POSTC), thalamo-parietal (T-PAR), thalamo-occipital (T-OCC), anterior thalamic radiation (ATR), superior thalamic radiation (STR), optic radiation (OR), fronto-pontine tract (FPT), cortico-spinal tract (CST), parieto-occipital pontine (POPT), corpus callosum I to VII (CC-I to CC-VII), anterior commissure (AC), cingulum (CG). We then assessed per study participant the fixel metrics per fiber tract by averaging the fiber density, fiber-bundle cross-section and fiber density cross-section of all fixels belonging to the respective fiber tract.

To assess regional associations between regional tau pathology and tract-specific fixel metrics in the AD sample, we determined regional tau-PET SUVRs in cortical projections of fiber tracts. To this end, we used masks from the beginning and ending of the fiber tracts, as obtained with TractSeg, intersected with a cortical gray matter mask. The regions of interest in FOD template space were brought to tau-PET images in MNI space by non-linear registration with Advanced Normalization Tools (ANTs)[50] to determine regional tau-PET SUVRs.

PET acquisition and processing

Amyloid-PET was recorded in 4x5min frames 50-70min after ^{18}F-florbetapir injection or 90-110min after ^{18}F-florbetaben injection.[25] Tau-PET was acquired 75-105min after injection of ^{18}F-

flortaucipir in 6x5min frames. All time frames were motion corrected and averaged to obtain mean images (for details see http://adni.loni.usc.edu/methods/pet-analysis-method/pet-analysis/). Structural T1-weighted MRI images were processed using the ANTs cortical thickness pipeline and parcellated with the Desikan-Killiany Atlas[51] and non-linearly registered to MNI-space.[52] Amyloid-PET and tau-PET images were co-registered via native-space T1-weighted images to MNI standard space using ANTs-derived normalization parameters. Global amyloid-PET SUVRs were intensity normalized to the whole cerebellum and transformed to centiloid.[53] Partial volume corrected global tau-PET SUVRs were obtained from the ADNI database, which were calculated using the inferior cerebellum as reference region and averaged across neocortical Desikan-Killiany atlas ROIs (see here for details: https://ida.loni.usc.edu/login.jsp). Partial volume correction was performed by ADNI PET Core at UC Berkeley, using the geometric transfer method. For regional tau-PET SUVRs, we employed a congruent approach, applying geometric transfer method-based partial volume correction for cortical projections of white matter fiber tracts (PETPVC toolbox: https://github.com/UCL/PETPVC[54]). Specifically, we used the geometric transfer matrix approach to correct the ROI-based tau-PET data for grey matter density using the segmented T1-weighted image that was obtained in closest proximity to the tau-PET scan.

Statistical Analyses

All statistical analyses were performed in R (version 3.6.1).[55] The statistical significance level was set at $\alpha < 0.05$.

To compare between controls and patients with respect to demographic characteristics, vascular risk factors, conventional MRI and PET markers, we used chi-squared (χ^2) tests (for categorical variables) and non-parametric Wilcoxon rank sum tests and Kruskal-Wallis tests (for continuous variables), as appropriate.

Next, we were interested in group differences in tract-specific fixel metrics between SVD and matched controls, and between groups with different biomarker status for AD (Aβ+T– vs. Aβ–T–; Aβ+T+ vs. Aβ–T– and Aβ+T+ vs. Aβ+T–). Since fixel metrics have been shown to be significantly influenced by head size,[56] we first regressed out the effect of intracranial volume and conducted subsequent analysis on residuals, i.e., fixel metrics corrected for head size ('stats'

package). We then calculated the effect size for group comparisons in all predefined fiber tracts using Cohen's d ('psych' package).

Next, we performed simple linear regression analyses to explore associations between SVD and AD typical imaging hallmarks (independent variable) and fiber density and fiber-bundle cross-section of the respective fiber tract (dependent variable, 'stats' package). For SVD hallmarks, we included white matter hyperintensity volume, lacune and cerebral microbleed count. For AD hallmarks, we included global amyloid-PET (centiloid), global tau-PET, regional tau-PET (i.e. tau-PET SUVR in cortical projections of the respective fiber tract). We also included normalized global brain volume indicative of neurodegeneration as an independent variable, which is associated with both AD[3] and SVD.[57] Additionally, we assessed associations with age to ensure that potential associations were not driven by aging alone. In these regression analyses, we used the full extent of the SVD and AD sample by also including the controls (but report sub-sequent sensitivity analyses in the CADASIL only and the Aβ+ only group in the Supplement). Effect sizes were determined by the adjusted R^2. *P*-values were adjusted with the false discovery rate (FDR) per sample and fixel metric resulting in a maximum of 5% of false positives.

To assess the relative variable importance of disease markers in explaining fixel metrics, we performed multivariable random forest regression analyses with conditional inference trees in the AD sample (R package 'party'). This machine-learning method overcomes the problem of multicollinearity within the disease markers. We focused on four variables of interest: WMHV as a marker for SVD, amyloid- and global tau-PET as a marker for AD and brain volume as a marker for neurodegeneration. We repeated random forest regression 100 times to determine the point estimate and a 95% confidence interval.

All analyses were conducted independently in each of the three samples.

Data availability

Anonymized data of the SVD and validation samples will be made available upon reasonable request to the corresponding author and only after permission of the regulatory bodies. ADNI data is freely available and can be retrieved from adni.loni.usc.edu upon registration to the ADNI database.

Results

Sample characteristics and demographics are shown in **Table 1**. As expected, SVD patients had higher WMH volumes, more lacunes and microbleeds compared to controls (p<0.001). SVD patients further had higher rates of hypercholesterolemia than age-matched controls (p<0.05). WMH volume increased with progressing amyloid and tau pathology in the AD sample (p<0.001).

Fixel metric group comparisons

Genetically defined SVD predominantly leads to reduced fiber density

The fiber density of all white matter fiber tracts was reduced in SVD compared to controls (range of Cohen's d[0.33;0.57], **Figure 4A&B**, **Supplementary Table e-2**). Results for the fiber-bundle cross-section were less consistent. While the fiber-bundle cross-section of most fiber tracts was reduced in SVD compared to controls (Cohen's d[0.19;0.35], 11 tracts showed no group difference and the fiber-bundle cross-section of the anterior thalamic radiation and the first segment of the corpus callosum (rostrum) was even higher in SVD compared to controls (Cohen's d=–0.33, both tracts).

Both fiber density and fiber-bundle cross-section are reduced across the AD spectrum

In the AD sample, the Aβ+T– group showed consistently lower fiber density in most fiber tracts compared to the Aβ–T– control group (Cohen's d[0.27;0.49], **Figure 4C&D**, **Supplementary Table e-3**). The fiber-bundle cross-section was also reduced in the Aβ+T– group (Cohen's d[0.27;0.51]). Similarly, the Aβ+T+ group showed lower fiber density (Cohen's d[0.30;0.43])

and lower fiber-bundle cross-section (Cohen's d[0.27;0.40]) compared to the Aβ–T– control group.

To determine the extent to which these effects were driven by differences in SVD burden between groups, we included WMH volume as covariate in a sensitivity analysis. This reduced effect sizes on average by 42% for fiber density and 8% for fiber-bundle cross-section (Aβ+T– vs. Aβ–T–), and by 21% for fiber density and 7% for fiber-bundle-cross section (Aβ+T+ vs. Aβ–T–, **Supplementary Table e-3**).

The Aβ+T+ group did not show any additional white matter damage regarding fiber density or fiber-bundle cross-section compared to Aβ+T–. In summary, both fiber density and fiber-bundle cross-section were reduced in the presence of amyloid pathology, but not further altered by additional tau pathology.

Associations with disease markers

Reduced fiber density is mainly associated with higher SVD burden

In simple linear regression in the SVD sample, fiber density of all fiber tracts was strongly associated with WMH volume (range of R^2_{adj}[0.29;0.79]), lacunes ($R^2_{adj.}$[0.12;0.48]), and microbleeds (R^2_{adj}[0.16;0.43], **Figure 5A**, **Supplementary Table e-4**). In contrast, effect sizes were small for associations with age (R^2_{adj}[0.03;0.13]) and brain volume (R^2_{adj}[0.05;0.16]) .

Fiber-bundle cross-section was also associated with WMH volume, but with smaller effect sizes (R^2_{adj}[0.06;0.43]), as well as with lacune count (R^2_{adj}[0.06;0.52]), microbleed count ($R^2_{adj.}$[0.07;0.38]) and brain volume ($R^2_{adj.}$[0.05;0.29]). Effect sizes were small for associations with age (age: $R^2_{adj.}$[0.04;0.13]).

Findings could be replicated when assessing associations in CADASIL patients only (**Supplementary Figure e-1A**).

Reduced fiber-bundle cross-section is mainly associated with cerebral atrophy in the AD sample

In simple linear regression analyses, fiber density in the AD sample was likewise associated with WMH volume ($R^2_{adj.}$[0.04;0.20], **Figure 5B**, **Supplementary Table e-5**) and to some extent with microbleed count ($R^2_{adj.}$[0.05;0.08]) but not with lacune count, which was expected given the low number of lacunes and microbleeds in this sample (**Table 1**). Fiber density was not associated with brain volume and with age only in selected fiber tracts ($R^2_{adj.}$[0.05;0.17]). Effect sizes for associations with AD PET markers were substantially smaller than with SVD MRI markers (amyloid-PET: $R^2_{adj.}$[0.04;0.11]) and tau-PET ($R^2_{adj.}$[0.04]).

Compared to fiber density, fiber-bundle cross-section was less associated with SVD imaging markers (WMHV: $R^2_{adj.}$[0.04;0.06]; no significant associations with lacunes or microbleeds). In contrast, fiber-bundle cross-section of all fiber tracts was strongly associated with brain volume ($R^2_{adj.}$[0.06;0.35]) and to some extent with age ($R^2_{adj.}$[0.04;0.20]). Associations with AD PET markers were mostly absent or showed only small effect sizes (amyloid-PET: $R^2_{adj.}$[0.04;0.05]; tau-PET: $R^2_{adj.}$[0.05;0.06]).

All findings could be replicated when assessing associations in Aβ+ study participants only, except for associations with AD PET markers, which were even weaker (**Supplementary Figure e-1B**).

In multivariable random forest regression analyses (**Figure 6**), WMH volume showed the highest variable importance for fiber density in most fiber tracts, while brain volume showed the highest variable importance for fiber bundle cross-section in all tracts.

Fiber density is associated with SVD markers and fiber-bundle cross-section with brain volume in presumed mixed pathology

Also in the validation sample, fiber density of all tracts was highly associated with WMH volume ($R^2_{adj.}$[0.08;0.48], **Figure 5C**, **Supplementary Table e-6**). Fiber density of all tracts was also (with smaller effect sizes) associated with lacune count ($R^2_{adj.}$[0.03;0.26]), microbleed count ($R^2_{adj.}$[0.04;0.15]), brain volume ($R^2_{adj.}$[0.01;0.19]) and age ($R^2_{adj.}$[0.03;0.23]).

Effect sizes were small for associations between fiber-bundle cross-section was only weakly associated with WMH volume ($R^2_{adj.}$[0.02;0.09]; lacune count ($R^2_{adj.}$[0.02;0.13]) and microbleed count ($R^2_{adj.}$[0.02;0.09]). Effect sizes were largest for brain volume ($R^2_{adj.}$[0.06;0.42]).

Results of group comparisons and associations with disease markers of the combined metric fiber density and bundle cross-section can be found in the Supplement as well as scatterplots of the most important findings (**Supplementary Figure e-2 to e-5).**

Discussion

Our multi-modal neuroimaging study systematically assessed the utility of fixel-based, tract-specific diffusion metrics to disentangle the effects of AD and SVD on white matter. Our main findings are that i) fiber density was markedly reduced in genetically defined SVD and showed the strongest association with SVD imaging hallmarks. ii) Fiber-bundle cross-section was mainly associated with brain volume, especially in the AD sample. iii) Both fiber density and fiber-bundle cross-section were reduced in the presence of amyloid, but this was not further exacerbated by abnormal tau deposition. Taken together, our results suggest that the white matter microstructure metric fiber density is primarily determined by SVD, while the macrostructure metric fiber-bundle cross-section is strongly associated with neurodegeneration. Importantly, the capability of fixel metrics to capture distinct effects of SVD and neurodegeneration was validated in an independent sample.

The marked reduction of the microscopic feature fiber density with increasing SVD burden might result from increased extracellular water moving axons further apart.[21] In line with this, we previously demonstrated that diffusion tensor imaging alterations in SVD are mainly determined by increases in extracellular free water.[58] In addition, a reduction in apparent fiber density (although not assessed using fixel-based analysis) has been suggested to accompany an increase in extracellular water within white matter hyperintensities of CADASIL patients.[59] Vascular edema, e.g. resulting from blood-brain-barrier leakage in SVD, might be a main driver of this fluid shift.[5,60] Interestingly, while the fiber density decreased, we observed in the genetically

defined SVD sample a simultaneous increase in the fiber-bundle cross-section of two tracts, the anterior thalamic radiation and the first segment of the corpus callosum (rostrum, harboring parts of the forceps minor). Strikingly, the anterior thalamic radiation and forceps minor were previously identified as strategic locations for processing speed performance in SVD,[61,62] the core cognitive deficit of the disease. One might speculate that the expansion of the extracellular space following vascular edema led to a swelling of these fiber tracts which is captured by an increase in fiber-bundle cross-section.[21,60]

The macroscopic feature fiber-bundle cross-section was most prominently reduced with increasing amyloid pathology in group comparisons and strongly associated with cerebral atrophy as a proxy of neurodegeneration in the AD and validation sample. Together with the finding that brain volume was not or only weakly associated with fiber density, this suggests that in fixel-based analysis, neurodegeneration predominantly manifests in alterations of white matter macrostructure, but not microstructure. Thus, fiber-bundle cross-section indeed seems to be reflective of the accumulated axon loss as previously postulated.[19]

While associations in the SVD sample were strongest for fiber density, and in the AD sample for fiber-bundle cross-section, both associations were found in the validation sample with mixed pathologies, supporting the concept that both SVD and AD contribute to white matter damage in mixed disease.

In the AD sample, both fiber density and fiber-bundle cross-section were reduced upon amyloid pathology in group comparisons, which might seem counterintuitive at first. As expected from epidemiological and histopathology studies,[6,7] concomitant SVD was found in the AD sample, with the largest difference in WMH burden between the A+T– group and matched A–T– controls. Controlling for this group difference in WMH volume attenuated the observed effects of amyloid, especially on fiber density. Thus, the effect of amyloid on fiber density can at least partly be explained by concomitant SVD, which is plausible given the likely presence of cerebral amyloid angiopathy, which is also captured by amyloid-PET.[63,64]

Brain atrophy clearly showed the strongest associations with fixel metrics, i.e. fiber-bund cross-section, in the AD sample. But in contrast to a previously postulated hypothesis,[44] we did not find that cortical tau pathology is a main driver of alterations in fixel metrics.

While many studies investigated white matter alterations in SVD or AD using models operating on the voxel level,[9] such as diffusion tensor imaging and more advanced diffusion models,[66] only very few studies have so far utilized fixel-based analysis. Importantly, none of the prior fixel-based studies considered mixed disease, but studied either SVD or AD in isolation, thus ignoring the crucial aspect of concomitant pathologies. Despite technical limitations,[21,67] it was recently shown that fiber density obtained from fixel-based analysis is highly sensitive towards processing speeds deficits in sporadic SVD,[68] confirming previous findings from voxel-based analysis. The aforementioned fixel-based analysis study in AD reported a reduction in both fiber density and fiber-bundle cross-section in MCI and AD patients.[22] However, besides not considering concomitant SVD, a full AD biomarker characterization was not possible due to prematurity of tau-PET tracers upon data collection of that study.[69] By considering both pathologies and by including data from both amyloid- and tau-PET, we were able to substantially extend previous results, close crucial knowledge gaps and to derive insights highly relevant for both future research studies and potentially also clinical applications.

Our study has some potential limitations. First, in the mixed pathology sample AD biomarkers were not available, precluding an independent validation of results for the direct effects of amyloid and tau pathology. Second, while all samples had diffusion MRI data suitable for fixel-based analysis, the acquisition was not harmonized across the three samples. However, this can also be regarded as a strength in terms of generalizability and independent validation of findings, because despite differences in the MRI acquisition, we found consistent results across all three samples. MRI data in the AD sample was acquired across 13 different scanners. Scanner effects were mitigated by selecting only acquisitions with identical parameters and an intensity normalization step. Eventually, excellent inter-site reproducibility of fixel metrics (**Supplementary Analysis**) enabled pooling of data from different scanners. Lastly, amyloid-PET data was not partial volume corrected due to centiloid transformation,[70] hence our results warrant further replication using a large single tracer dataset.

A main strength of this study is the extensive biomarker characterization, including multiple markers for SVD as well as amyloid- and tau-PET data in the AD sample. This enabled a multi-modal approach, which was deemed essential in further validation of fixel-based metrics by the developers of the method.[21] Unlike in the AD field, truly SVD-specific biomarkers are still

lacking. To overcome this limitation, we included the sample of genetically defined SVD patients. Since these patients were relatively young, concomitant AD and other age-related neurodegenerative pathology can be regarded as rare, thus enabling the unique opportunity to study pure SVD without the need for biomarker characterization. While data from autosomal dominant AD would have perfectly complemented our analysis in this regard, we are not aware of any familial AD studies with diffusion MRI data suitable for fixel-based analysis.

The ability of the fixel-based analysis to identify distinct effects of SVD and neurodegeneration on white matter opens a path towards personalized medicine. Future work should address the ability of fixel-derived diffusion markers to explain the extent to which SVD and neurodegeneration contribute to cognitive impairment in mixed disease. This would enable disease-specific interventions targeting AD- or SVD-related brain alterations rather than managing disease-shared risk factors. Our results illustrate once more that it is mandatory to consider SVD when assessing white matter integrity in the context of dementia studies and trials. Furthermore, longitudinal studies are required to capture temporal dynamics of fiber density and fiber-bundle cross-section. Given recent indications for SVD lesion regression,[71] it remains to be assessed whether the reduction in fiber density observed in SVD is irreversible and how it changes upon disease intervention, e.g., intensified risk factor treatment. Technical validation studies, assessing test-retest reliability and inter-site reproducibility of these novel markers in patients, will be essential for developing a surrogate endpoint for clinical trials.

In conclusion, our results show that fiber density and fiber-bundle cross-section, obtained from fixel-based analysis of diffusion MRI data, allow to identify distinct effects of SVD and neurodegeneration on white matter integrity. While white matter microstructure is predominantly determined by SVD, neurodegeneration leads to alterations in white matter macrostructure. Leveraging these distinct effects, fixel-based white matter analysis can propel future research, clinical trials targeting disease-specific mechanisms and clinical applications in the context of precision medicine.

Acknowledgements

Data used in preparation of this article were obtained from the Munich cohort of the ZOOM@SVDs study, which is part of the SVDs@target project. As such, the investigators within the ZOOM@SVDs study contributed to the design but did not participate in analysis or writing of this report. Data used in preparation of this article were obtained from the Alzheimer's Disease Neuroimaging Initiative (ADNI) database (adni.loni.usc.edu). As such, the investigators within the ADNI contributed to the design and implementation of ADNI and/or provided data but did not participate in analysis or writing of this report. A complete listing of ADNI investigators can be found at: http://adni.loni.usc.edu/wp-content/uploads/how_to_apply/ADNI_Acknowledgement_List.pdf

Funding

This project has received funding from the European Union's Horizon 2020 research and innovation programme No 666881, SVDs@target (to M Dichgans), the DFG as part of the Munich Cluster for Systems Neurology (EXC 2145 SyNergy – ID 390857198), and the Vascular Dementia Research Foundation.
M Cai was supported by China Scholarship Council (201706100189). AM Tuladhar is a junior staff member of the Dutch Heart Foundation (grant number 2016T044).

Data collection and sharing for this project was funded by the Alzheimer's Disease Neuroimaging Initiative (ADNI) (National Institutes of Health Grant U01 AG024904) and DOD ADNI (Department of Defense award number W81XWH-12-2-0012). ADNI is funded by the National Institute on Aging, the National Institute of Biomedical Imaging and Bioengineering, and through generous contributions from the following: AbbVie, Alzheimer's Association; Alzheimer's Drug Discovery Foundation; Araclon Biotech; BioClinica, Inc.; Biogen; Bristol-Myers Squibb Company; CereSpir, Inc.; Cogstate; Eisai Inc.; Elan Pharmaceuticals, Inc.; Eli Lilly and Company; EuroImmun; F. Hoffmann-La Roche Ltd and its affiliated company Genentech, Inc.; Fujirebio; GE Healthcare; IXICO Ltd.; Janssen Alzheimer Immunotherapy

Research & Development, LLC.; Johnson & Johnson Pharmaceutical Research & Development LLC.; Lumosity; Lundbeck; Merck & Co., Inc.; Meso Scale Diagnostics, LLC.; NeuroRx Research; Neurotrack Technologies; Novartis Pharmaceuticals Corporation; Pfizer Inc.; Piramal Imaging; Servier; Takeda Pharmaceutical Company; and Transition Therapeutics. The Canadian Institutes of Health Research is providing funds to support ADNI clinical sites in Canada. Private sector contributions are facilitated by the Foundation for the National Institutes of Health (www.fnih.org). The grantee organization is the Northern California Institute for Research and Education, and the study is coordinated by the Alzheimer's Therapeutic Research Institute at the University of Southern California. ADNI data are disseminated by the Laboratory for Neuro Imaging at the University of Southern California.

Competing interests

The authors report no competing interests.

Supplementary material

Supplementary material is available at *Brain* online.

References

1. van der Flier WM, Skoog I, Schneider JA, et al. Vascular cognitive impairment. *Nat Rev Dis Primer*. 2018;4(1):1-16. doi:10.1038/nrdp.2018.3

2. Dichgans M, Leys D. Vascular Cognitive Impairment. *Circ Res*. 2017;120(3):573-591. doi:10.1161/CIRCRESAHA.116.308426

3. Jack CR, Bennett DA, Blennow K, et al. NIA-AA Research Framework: Toward a biological definition of Alzheimer's disease. *Alzheimers Dement*. 2018;14(4):535-562. doi:10.1016/j.jalz.2018.02.018

4. Wardlaw JM, Smith EE, Biessels GJ, et al. Neuroimaging standards for research into small vessel disease and its contribution to ageing and neurodegeneration. *Lancet Neurol*. 2013;12(8):822-838. doi:10.1016/S1474-4422(13)70124-8

5. Wardlaw JM, Smith C, Dichgans M. Small vessel disease: mechanisms and clinical implications. *Lancet Neurol*. 2019;18(7):684-696. doi:10.1016/S1474-4422(19)30079-1

6. Kapasi A, DeCarli C, Schneider JA. Impact of Multiple Pathologies on the Threshold for Clinically Overt Dementia. *Acta Neuropathol (Berl)*. 2017;134(2):171-186. doi:10.1007/s00401-017-1717-7

7. Attems J, Jellinger KA. The overlap between vascular disease and Alzheimer's disease - lessons from pathology. *BMC Med*. 2014;12(1):1-12. doi:10.1186/s12916-014-0206-2

8. Beach TG, Malek-Ahmadi M. Alzheimer's Disease Neuropathological Comorbidities are Common in the Younger-Old. *J Alzheimers Dis*. 2021;79(1):389-400. doi:10.3233/JAD-201213

9. Raja R, Rosenberg G, Caprihan A. Review of diffusion MRI studies in chronic white matter diseases. *Neurosci Lett*. 2019;694:198-207. doi:10.1016/j.neulet.2018.12.007

10. Baykara E, Gesierich B, Adam R, et al. A Novel Imaging Marker for Small Vessel Disease Based on Skeletonization of White Matter Tracts and Diffusion Histograms. *Ann Neurol*. 2016;80(4):581-592. doi:https://doi.org/10.1002/ana.24758

11. Pichet Binette A, Theaud G, Rheault F, et al. Bundle-specific associations between white matter microstructure and Aβ and tau pathology in preclinical Alzheimer's disease. *eLife*. 2021;10:e62929. doi:10.7554/eLife.62929

12. Nasrabady SE, Rizvi B, Goldman JE, Brickman AM. White matter changes in Alzheimer's disease: a focus on myelin and oligodendrocytes. *Acta Neuropathol Commun*. 2018;6(1):22. doi:10.1186/s40478-018-0515-3

13. Finsterwalder S, Vlegels N, Gesierich B, et al. Small vessel disease more than Alzheimer's disease determines diffusion MRI alterations in memory clinic patients. *Alzheimers Dement*. 2020;16(11):1504-1514. doi:10.1002/alz.12150

14. Vemuri P, Lesnick TG, Knopman DS, et al. Amyloid, Vascular, and Resilience Pathways Associated with Cognitive Aging. *Ann Neurol*. 2019;86(6):866-877. doi:10.1002/ana.25600

15. Raghavan S, Przybelski SA, Reid RI, et al. White matter damage due to vascular, tau, and TDP-43 pathologies and its relevance to cognition. *Acta Neuropathol Commun*. 2022;10(1):16. doi:10.1186/s40478-022-01319-6

16. Jones DK, Knösche TR, Turner R. White matter integrity, fiber count, and other fallacies: The do's and don'ts of diffusion MRI. *NeuroImage*. 2013;73:239-254. doi:10.1016/j.neuroimage.2012.06.081

17. Tournier JD, Calamante F, Connelly A. MRtrix: Diffusion tractography in crossing fiber regions. *Int J Imaging Syst Technol*. 2012;22(1):53-66. doi:https://doi.org/10.1002/ima.22005

18. Jeurissen B, Leemans A, Tournier JD, Jones DK, Sijbers J. Investigating the prevalence of complex fiber configurations in white matter tissue with diffusion magnetic resonance imaging. *Hum Brain Mapp*. 2013;34(11):2747-2766.

19. Raffelt DA, Tournier JD, Smith RE, et al. Investigating white matter fibre density and morphology using fixel-based analysis. *NeuroImage*. 2017;144:58-73. doi:10.1016/j.neuroimage.2016.09.029

20. Raffelt D, Tournier JD, Rose S, et al. Apparent Fibre Density: A novel measure for the analysis of diffusion-weighted magnetic resonance images. *NeuroImage*. 2012;59(4):3976-3994. doi:10.1016/j.neuroimage.2011.10.045

21. Dhollander T, Clemente A, Singh M, et al. Fixel-based Analysis of Diffusion MRI: Methods, Applications, Challenges and Opportunities. *NeuroImage*. 2021;241:118417. doi:10.1016/j.neuroimage.2021.118417

22. Mito R, Raffelt D, Dhollander T, et al. Fibre-specific white matter reductions in Alzheimer's disease and mild cognitive impairment. *Brain*. 2018;141(3):888-902. doi:10.1093/brain/awx355

23. van den Brink H, Kopczak A, Arts T, et al. Zooming in on cerebral small vessel function in small vessel diseases with 7T MRI: Rationale and design of the "ZOOM@SVDs" study. *Cereb Circ - Cogn Behav*. 2021;2:100013. doi:10.1016/j.cccb.2021.100013

24. Weiner MW, Veitch DP, Aisen PS, et al. The Alzheimer's Disease Neuroimaging Initiative 3: Continued innovation for clinical trial improvement. *Alzheimers Dement*. 2017;13(5):561-571. doi:10.1016/j.jalz.2016.10.006

25. Landau SM, Mintun MA, Joshi AD, et al. Amyloid Deposition, Hypometabolism, and Longitudinal Cognitive Decline. *Ann Neurol*. 2012;72(4):578-586. doi:10.1002/ana.23650

26. Biel D, Brendel M, Rubinski A, et al. Tau-PET and in vivo Braak-staging as prognostic markers of future cognitive decline in cognitively normal to demented individuals. *Alzheimers Res Ther*. 2021;13(1):137. doi:10.1186/s13195-021-00880-x

27. Schöll M, Lockhart SN, Schonhaut DR, et al. PET Imaging of Tau Deposition in the Aging Human Brain. *Neuron*. 2016;89(5):971-982. doi:10.1016/j.neuron.2016.01.028

28. van Norden AG, de Laat KF, Gons RA, et al. Causes and consequences of cerebral small vessel disease. The RUN DMC study: a prospective cohort study. Study rationale and protocol. *BMC Neurol*. 2011;11(1):29. doi:10.1186/1471-2377-11-29

29. Tuladhar AM, van Uden IWM, Rutten-Jacobs LCA, et al. Structural network efficiency predicts conversion to dementia. *Neurology*. 2016;86(12):1112-1119. doi:10.1212/WNL.0000000000002502

30. Andersson JLR, Skare S, Ashburner J. How to correct susceptibility distortions in spin-echo echo-planar images: application to diffusion tensor imaging. *NeuroImage*. 2003;20(2):870-888. doi:10.1016/S1053-8119(03)00336-7

31. Smith SM, Jenkinson M, Woolrich MW, et al. Advances in functional and structural MR image analysis and implementation as FSL. *NeuroImage*. 2004;23:S208-S219. doi:10.1016/j.neuroimage.2004.07.051

32. Andermatt S, Pezold S, Cattin PC. Automated Segmentation of Multiple Sclerosis Lesions Using Multi-dimensional Gated Recurrent Units. In: Crimi A, Bakas S, Kuijf H, Menze B, Reyes M, eds. *Brainlesion: Glioma, Multiple Sclerosis, Stroke and Traumatic Brain Injuries*. Lecture Notes in Computer Science. Springer International Publishing; 2018:31-42. doi:10.1007/978-3-319-75238-9_3

33. Puonti O, Iglesias JE, Van Leemput K. Fast and sequence-adaptive whole-brain segmentation using parametric Bayesian modeling. *NeuroImage*. 2016;143:235-249. doi:10.1016/j.neuroimage.2016.09.011

34. ter Telgte A, Wiegertjes K, Tuladhar AM, et al. Investigating the origin and evolution of cerebral small vessel disease: The RUN DMC – InTENse study. *Eur Stroke J*. 2018;3(4):369-378. doi:10.1177/2396987318776088

35. Dewenter A, Gesierich B, ter Telgte A, et al. Systematic validation of structural brain networks in cerebral small vessel disease. *J Cereb Blood Flow Metab*. Published online Dezember 2021:0271678X211069228. doi:10.1177/0271678X211069228

36. Veraart J, Novikov DS, Christiaens D, Ades-aron B, Sijbers J, Fieremans E. Denoising of diffusion MRI using random matrix theory. *NeuroImage*. 2016;142:394-406. doi:10.1016/j.neuroimage.2016.08.016

37. Veraart J, Fieremans E, Novikov DS. Diffusion MRI noise mapping using random matrix theory. *Magn Reson Med*. 2016;76(5):1582-1593. doi:10.1002/mrm.26059

38. Cordero-Grande L, Christiaens D, Hutter J, Price AN, Hajnal JV. Complex diffusion-weighted image estimation via matrix recovery under general noise models. *NeuroImage*. 2019;200:391-404. doi:10.1016/j.neuroimage.2019.06.039

39. Tournier JD, Smith R, Raffelt D, et al. MRtrix3: A fast, flexible and open software framework for medical image processing and visualisation. *NeuroImage*. 2019;202:116137. doi:10.1016/j.neuroimage.2019.116137

40. Kellner E, Dhital B, Kiselev VG, Reisert M. Gibbs-ringing artifact removal based on local subvoxel-shifts. *Magn Reson Med*. 2016;76(5):1574-1581. doi:10.1002/mrm.26054

41. Andersson JLR, Sotiropoulos SN. An integrated approach to correction for off-resonance effects and subject movement in diffusion MR imaging. *NeuroImage*. 2016;125:1063-1078. doi:10.1016/j.neuroimage.2015.10.019

42. Andersson JLR, Graham MS, Zsoldos E, Sotiropoulos SN. Incorporating outlier detection and replacement into a non-parametric framework for movement and distortion correction of diffusion MR images. *NeuroImage*. 2016;141:556-572. doi:10.1016/j.neuroimage.2016.06.058

43. Andersson JLR, Graham MS, Drobnjak I, Zhang H, Filippini N, Bastiani M. Towards a comprehensive framework for movement and distortion correction of diffusion MR images: Within volume movement. *NeuroImage*. 2017;152:450-466. doi:10.1016/j.neuroimage.2017.02.085

44. Andersson JLR, Graham MS, Drobnjak I, Zhang H, Campbell J. Susceptibility-induced distortion that varies due to motion: Correction in diffusion MR without acquiring additional data. *NeuroImage*. 2018;171:277-295. doi:10.1016/j.neuroimage.2017.12.040

45. Schilling KG, Blaber J, Hansen C, et al. Distortion correction of diffusion weighted MRI without reverse phase-encoding scans or field-maps. *PLOS ONE*. 2020;15(7):e0236418. doi:10.1371/journal.pone.0236418

46. Schilling KG, Blaber J, Huo Y, et al. Synthesized b0 for diffusion distortion correction (Synb0-DisCo). *Magn Reson Imaging*. 2019;64:62-70. doi:10.1016/j.mri.2019.05.008

47. Jeurissen B, Tournier JD, Dhollander T, Connelly A, Sijbers J. Multi-tissue constrained spherical deconvolution for improved analysis of multi-shell diffusion MRI data. *NeuroImage*. 2014;103:411-426. doi:10.1016/j.neuroimage.2014.07.061

48. Dhollander T, Mito R, Raffelt D, Connelly A. Improved white matter response function estimation for 3-tissue constrained spherical deconvolution. In: ; 2019.

49. Wasserthal J, Neher P, Maier-Hein KH. TractSeg - Fast and accurate white matter tract segmentation. *NeuroImage*. 2018;183:239-253. doi:10.1016/j.neuroimage.2018.07.070

50. Avants BB, Tustison NJ, Song G, Cook PA, Klein A, Gee JC. A Reproducible Evaluation of ANTs Similarity Metric Performance in Brain Image Registration. *NeuroImage*. 2011;54(3):2033-2044. doi:10.1016/j.neuroimage.2010.09.025

51. Desikan RS, Ségonne F, Fischl B, et al. An automated labeling system for subdividing the human cerebral cortex on MRI scans into gyral based regions of interest. *NeuroImage*. 2006;31(3):968-980. doi:10.1016/j.neuroimage.2006.01.021

52. Tustison NJ, Cook PA, Klein A, et al. Large-scale evaluation of ANTs and FreeSurfer cortical thickness measurements. *NeuroImage*. 2014;99:166-179. doi:10.1016/j.neuroimage.2014.05.044

53. Klunk WE, Koeppe RA, Price JC, et al. The Centiloid Project: Standardizing Quantitative Amyloid Plaque Estimation by PET. *Alzheimers Dement J Alzheimers Assoc*. 2015;11(1):1-15.e4. doi:10.1016/j.jalz.2014.07.003

54. Thomas BA, Cuplov V, Bousse A, et al. PETPVC: a toolbox for performing partial volume correction techniques in positron emission tomography. *Phys Med Biol*. 2016;61(22):7975-7993. doi:10.1088/0031-9155/61/22/7975

55. R Core Team. R: A language and environment for statistical computing. *Vienna R Found Stat Comput*. Published online 2016.

56. Smith R, Dhollander T, Connelly A. *On the Regression of Intracranial Volume in Fixel-Based Analysis*.; 2019.

57. Smith EE, Biessels GJ, De Guio F, et al. Harmonizing brain magnetic resonance imaging methods for vascular contributions to neurodegeneration. *Alzheimers Dement Diagn Assess Dis Monit*. 2019;11:191-204. doi:10.1016/j.dadm.2019.01.002

58. Duering M, Finsterwalder S, Baykara E, et al. Free water determines diffusion alterations and clinical status in cerebral small vessel disease. *Alzheimers Dement J Alzheimers Assoc*. 2018;14(6):764-774. doi:10.1016/j.jalz.2017.12.007

59. Yu X, Yin X, Hong H, et al. Increased extracellular fluid is associated with white matter fiber degeneration in CADASIL: in vivo evidence from diffusion magnetic resonance imaging. *Fluids Barriers CNS*. 2021;18:29. doi:10.1186/s12987-021-00264-1

60. De Guio F, Mangin JF, Duering M, Ropele S, Chabriat H, Jouvent E. White matter edema at the early stage of cerebral autosomal-dominant arteriopathy with subcortical infarcts and leukoencephalopathy. *Stroke*. 2015;46(1):258-261. doi:10.1161/STROKEAHA.114.007018

61. Duering M, Gesierich B, Seiler S, et al. Strategic white matter tracts for processing speed deficits in age-related small vessel disease. *Neurology*. 2014;82(22):1946-1950. doi:10.1212/WNL.0000000000000475

62. Duering M, Zieren N, Hervé D, et al. Strategic role of frontal white matter tracts in vascular cognitive impairment: a voxel-based lesion-symptom mapping study in CADASIL. *Brain J Neurol*. 2011;134(Pt 8):2366-2375. doi:10.1093/brain/awr169

63. Charidimou A, Farid K, Baron JC. Amyloid-PET in sporadic cerebral amyloid angiopathy: A diagnostic accuracy meta-analysis. *Neurology*. 2017;89(14):1490-1498. doi:10.1212/WNL.0000000000004539

64. Gurol ME, Becker JA, Fotiadis P, et al. Florbetapir-PET to diagnose cerebral amyloid angiopathy. *Neurology*. 2016;87(19):2043-2049. doi:10.1212/WNL.0000000000003197

65. McAleese KE, Walker L, Colloby SJ, et al. Cortical tau pathology: a major player in fibre-specific white matter reductions in Alzheimer's disease? *Brain*. 2018;141(6):e44-e44. doi:10.1093/brain/awy084

66. Konieczny MJ, Dewenter A, Telgte A ter, et al. Multi-shell Diffusion MRI Models for White Matter Characterization in Cerebral Small Vessel Disease. *Neurology*. 2021;96(5):e698-e708. doi:10.1212/WNL.0000000000011213

67. Genc S, Tax CMW, Raven EP, Chamberland M, Parker GD, Jones DK. Impact of b-value on estimates of apparent fibre density. *Hum Brain Mapp*. 2020;41(10):2583-2595. doi:https://doi.org/10.1002/hbm.24964

68. Petersen M, Frey BM, Mayer C, et al. Fixel based analysis of white matter alterations in early stage cerebral small vessel disease. *Sci Rep*. 2022;12(1):1581. doi:10.1038/s41598-022-05665-2

69. Mito R, Raffelt D, Dhollander T, et al. Reply: Cortical tau pathology: a major player in fibre-specific white matter reductions in Alzheimer's disease? *Brain*. 2018;141(6):e45-e45. doi:10.1093/brain/awy086

70. La Joie R, Visani AV, Baker SL, et al. Prospective longitudinal atrophy in Alzheimer's disease correlates with the intensity and topography of baseline tau-PET. *Sci Transl Med*. 2020;12(524):eaau5732. doi:10.1126/scitranslmed.aau5732

71. van Leijsen EMC, de Leeuw FE, Tuladhar AM. Disease progression and regression in sporadic small vessel disease-insights from neuroimaging. *Clin Sci Lond Engl 1979*. 2017;131(12):1191-1206. doi:10.1042/CS20160384

Figure Legends

Figure 1 Illustration of fixel-based analysis of two exemplary crossing white matter fiber tracts (superior longitudinal fasciculus II in green, cortico-spinal tract in blue). A fixel corresponds to a specific fiber population per voxel. The depicted voxel harbors two fiber populations (color-coded per tract). A reduction in fiber density (with preserved fiber-bundle cross-section) is depicted on the left, while a reduction in fiber-bundle cross-section (with preserved fiber density) is depicted on the right.

Figure 2 Participant selection flowchart. Samples included genetically defined cerebral small vessel disease (CADASIL) and matched healthy controls (SVD sample), the full spectrum of Alzheimer's disease (AD) and a validation sample with presumed mixed pathology. ADD = Alzheimer's disease dementia, FoV = field of view, VD = vascular dementia.

Figure 3 Sagittal view of investigated white matter fiber tracts. Tracts generated in fiber orientation distribution template space are shown for illustration. We analyzed 29 white matter fiber tracts (only left hemisphere shown): AF = arcuate fasciculus, UF = uncinate fasciculus, IFOF = inferior fronto-occipital fasciculus, MLF = middle longitudinal fasciculus, ILF = inferior longitudinal fasciculus, SLF-I to SLF-III = superior longitudinal fasciculus I to III, T-PREF = thalamo-prefrontal, T-PREM = thalamo-premotor, T-PREC = thalamo-precentral, T-POSTC = thalamo-postcentral, T-PAR = thalamo-parietal, T-OCC = thalamo-occipital, ATR = anterior thalamic radiation, STR = superior thalamic radiation, OR = optic radiation, FPT = fronto-pontine tract, CST = cortico-spinal tract, POPT = parieto-occipital pontine, CC-I to CC-VII = corpus callosum I to VII (CC-I: Rostrum, CC-II: Genu, CC-III: Rostral body [premotor], CC-IV: Anterior midbody [primary motor], CC-V: Posterior midbody [primary somatosensory], CC-VI = Isthmus, CC-VII: Splenium), AC = anterior commissure, CG = cingulum.

Figure 4 Group comparisons of fixel metrics. (**A**) Difference in fixel metrics between age-matched healthy controls (HC) and CADASIL patients in the SVD sample quantified with Cohen's d represented by color. Circle size depicts statistical significance level. (**B**) Violin plots of fixel metrics of four representative fiber tracts in the SVD sample for exemplary

illustration. (**C**) Difference in fixel metrics between age-matched Aβ–T– and Aβ+T–; Aβ–T– and Aβ+T+; Aβ+T– and Aβ+T+ quantified with Cohen's d represented by color. Circle size depicts statistical significance level. (**D**) Violin plots of fixel metrics of the same four tracts in the AD sample. Please refer to **Figure 3** for abbreviations of the fiber tracts.

Figure 5 Associations with disease markers. Effect sizes (adj. R^2) obtained from simple linear regression analyses are represented by color. Circle size depicts statistical significance level. Associations between fixel metrics of white matter fiber tracts and disease markers were assessed in (**A**) the SVD sample, (**B**) the AD sample – including in addition amyloid-PET and tau-PET markers – and (**C**) the validation sample. Please refer to **Figure 3** for abbreviations of the fiber tracts. WMHV = white matter hyperintensity volume, BrainV = brain volume.

Figure 6 Multivariable random forest regression analyses for estimating the relative variable importance for the SVD marker white matter hyperintensity volume (WMHV, blue), markers of primary Alzheimer's disease pathology (orange) and brain volume (BrainV, red) with regard to tract-specific fixel metrics in the AD sample. Plots indicate point estimate and 95% confidence interval for the conditional variable importance. Please refer to **Figure 3** for abbreviations of the fiber tracts.

Table 1 Sample characteristics

	SVD			AD				Validation
	Control (*n*=22)	CADASIL (*n*=73)	*p-value*	Aβ−T− (*n*=34)	Aβ+T− (*n*=19)	Aβ+T+ (*n*=18)	*p-value*	(*n*=221)
Demographic characteristics								
Age [years], median (IQR)	60 (21.5)	55 (14)	0.2084	72.50 (9.5)	78.70 (7.8)	75.05 (6.85)	0.1359	73.64 (9.67)
Female, *n* (%)	9 (41)	44 (60)	0.1744	19 (56)	10 (53)	8 (44)	0.7335	98 (44)
Vascular risk factors, *n* (%)								
Hypertension	5 (23)	17 (23)	1.0	10 (29)	9 (47)	10 (56)	0.1506	146 (66)
Hypercholesterolemia	5 (23)	37 (51)	0.0471	9 (26)	3 (16)	8 (44)	0.1463	116 (52)
Diabetes	0 (0)	1 (0.01)	1.0	3 (9)	2 (11)	4 (22)	0.3647	33 (15)
Current or past smoking	9 (41)	44 (60)	0.2425	2 (6)	3 (16)	2 (11)	0.4994	143 (65)
PET markers, median (IQR)								
Amyloid-PET centiloid	-	-	-	−7.25 (11.91)	51.53 (38.26)	87.53 (46.41)	<0.0001	-
Global Tau-PET SUVR	-	-	-	1.03 (0.12)	1.08 (0.10)	1.18 (0.30)	<0.0001	-
MRI markers, median (IQR)								
WMH volume[a] [%]	0.03 (0.08)	4.58 (5.23)	<0.0001	0.24 (0.33)	0.53 (0.73)	0.69 (0.74)	0.0043	0.30 (0.69)
Lacune count	0 (0)	2 (7)	<0.0001	0 (0)	0 (0)	0 (0)	0.8763	0 (0)
Microbleed count	0 (0)	2 (7)	<0.0001	0 (0)	0 (0)	0 (0)	0.0160	0 (1)
Brain volume[a] [%]	75.72 (7.64)	76.22 (8.46)	0.2024	70.79 (1.27)	70.00 (2.55)	70.31 (3.26)	0.4158	74.34 (5.65)

Abbreviations: IQR = interquartile range; n = number; WMH = white matter hyperintensity.

[a] Normalized to the intracranial volume.

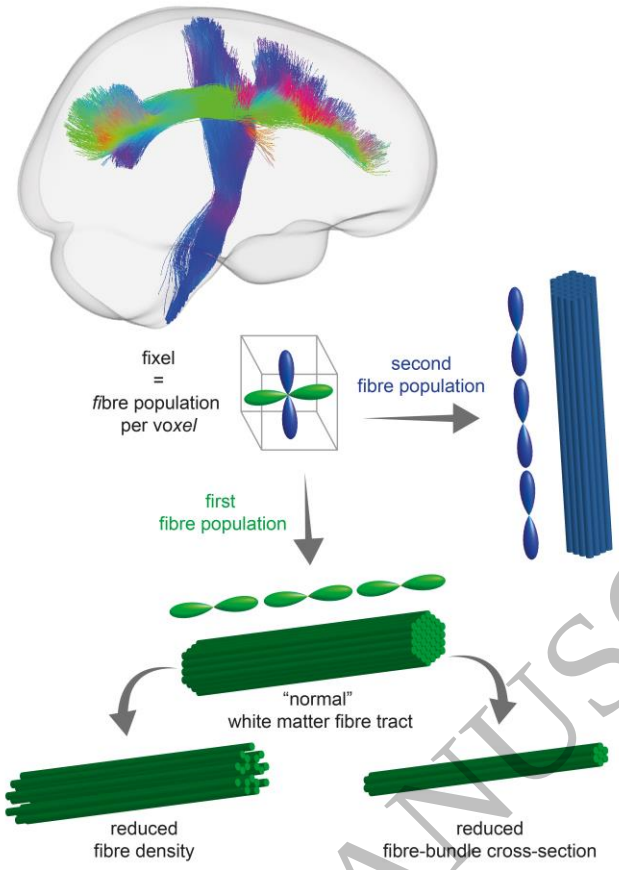

Figure 1
85x116 mm (.65 x DPI)

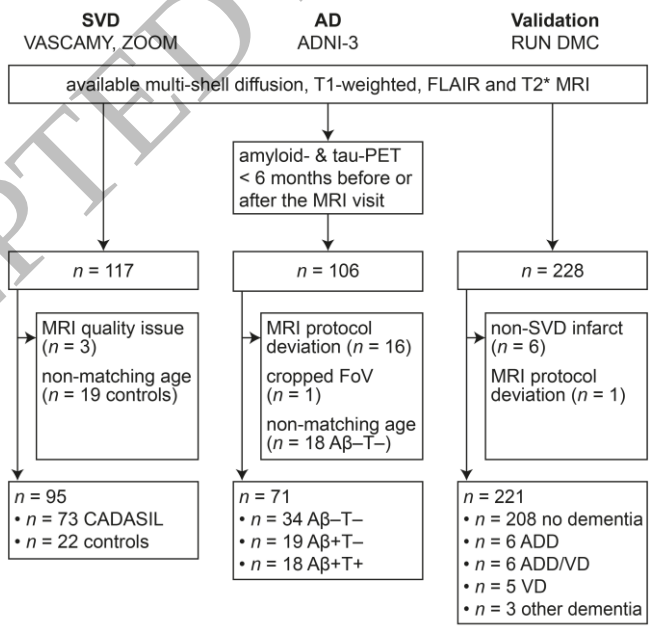

Figure 2
85x83 mm (.65 x DPI)

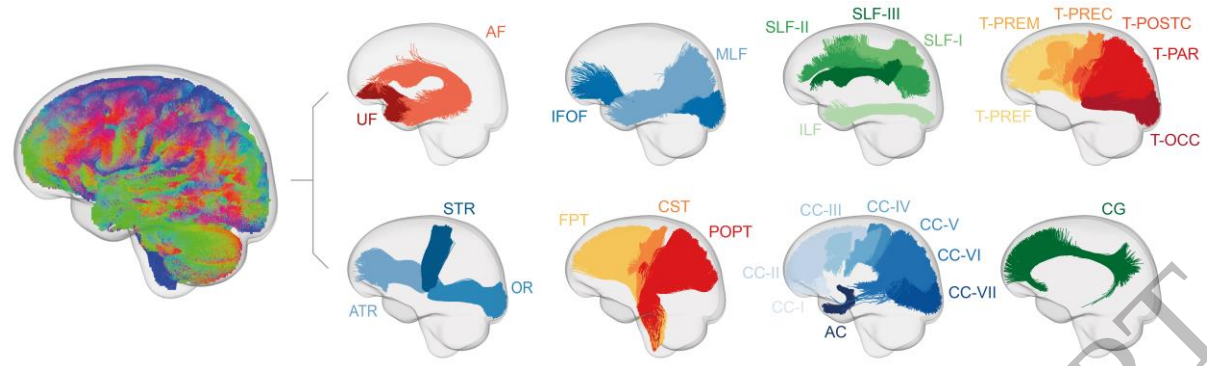

Figure 3
159x49 mm (.65 x DPI)

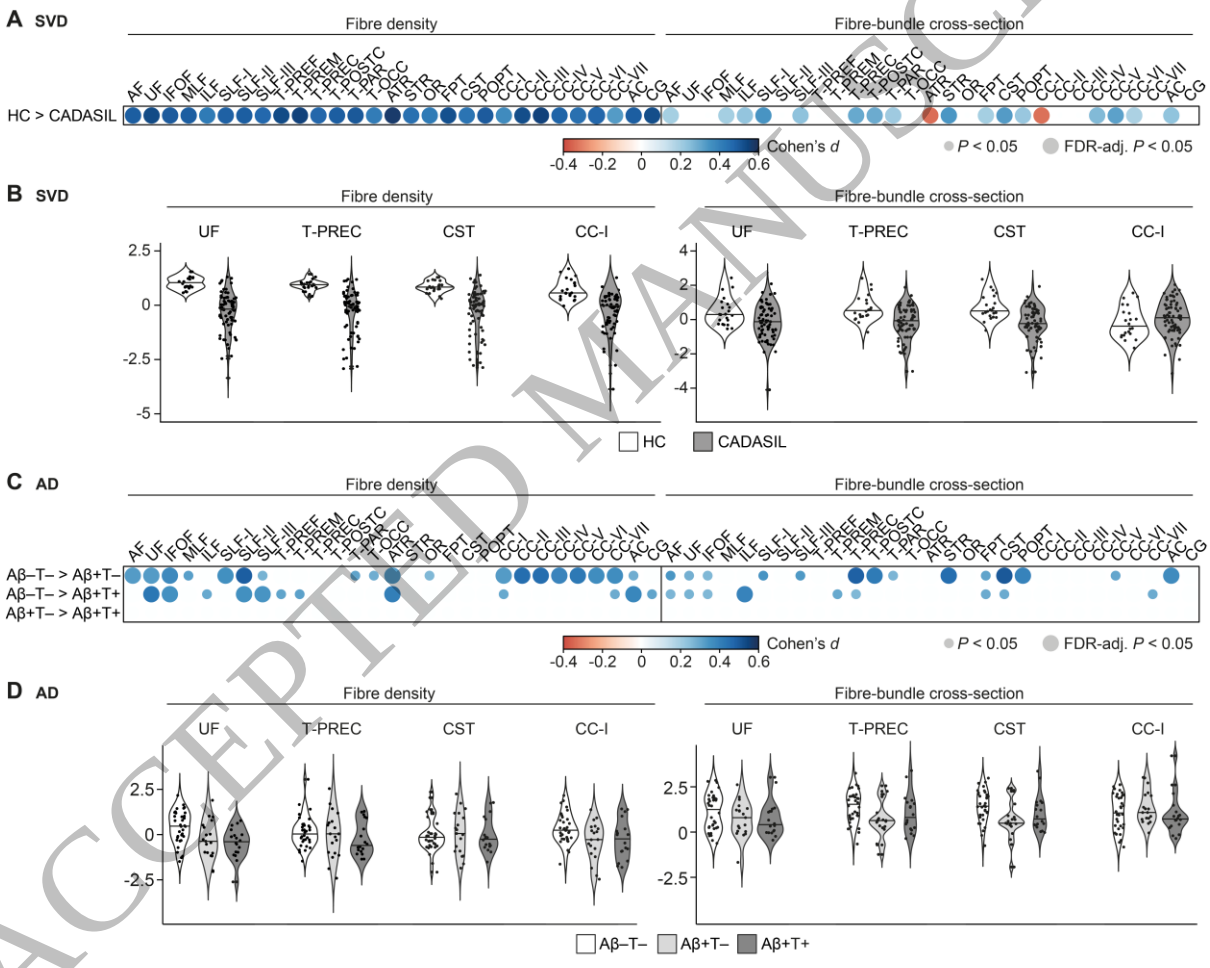

Figure 4
159x126 mm (.65 x DPI)

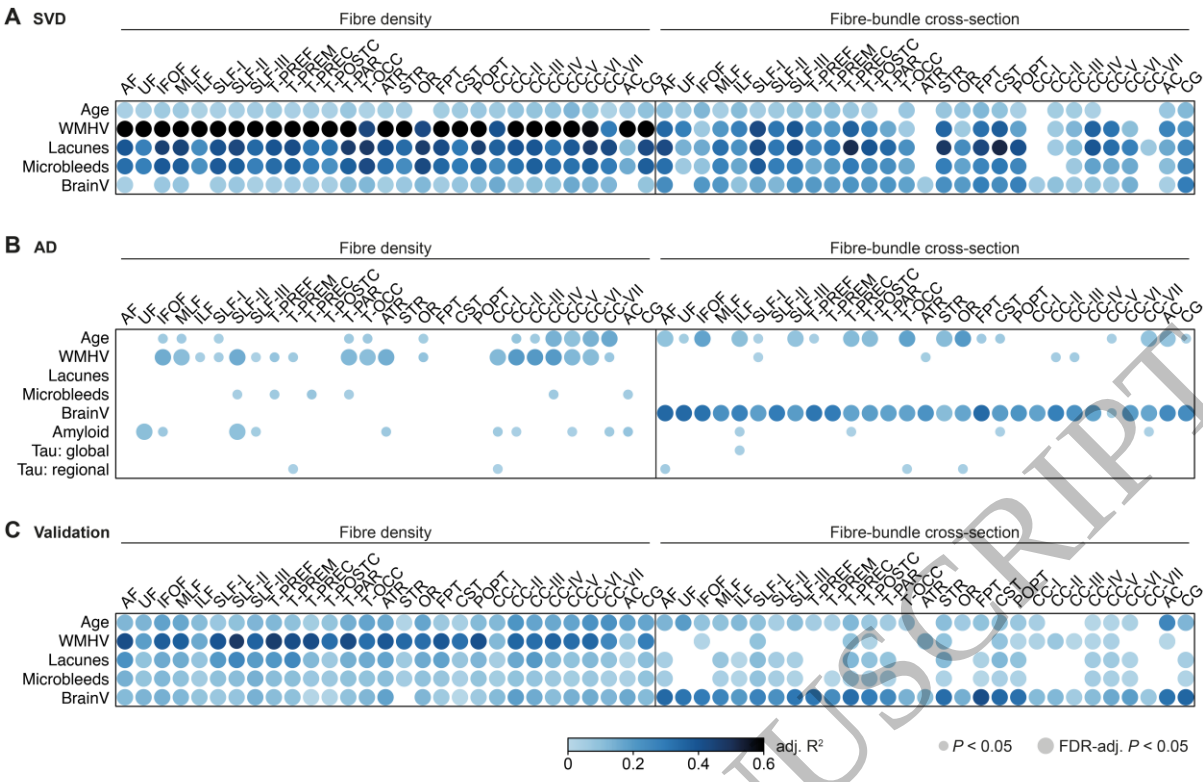

Figure 5
159x104 mm (.65 x DPI)

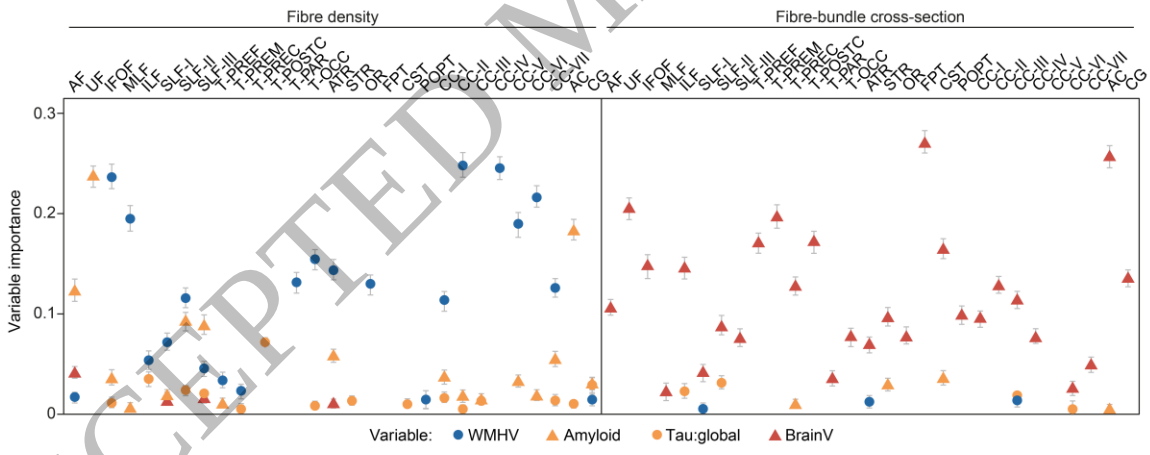

Figure 6
159x59 mm (.65 x DPI)